Characterization of reaction wheel micro-vibrations

W. De Munter[1], T. Delabie[1], D. Vandepitte[1]
[1] KU Leuven, Department Mechanical Engineering
Celestijnenlaan 300 B, B-3001, Heverlee, Belgium
e-mail: **wim.demunter@kuleuven.be**

Abstract
Reaction wheels are considered to be the largest contributors of vibrations on board a spacecraft. In order to estimate the effect on the pointing stability, the reaction wheel micro-vibrations have to be characterized first. In this paper, the micro-vibrations of two of the reaction wheels designed and developed at the KU Leuven, are modelled and tested. The micro-vibration model allows to predict the resonance modes of the reaction wheel assembly and the imbalances. These characteristics can then be verified by a dedicated micro-vibration test. The results of the micro-vibration tests showed that one of the wheels has a significant misalignment and a loose part in the assembly, while the other wheel showed the expected first harmonic to have the largest amplitude due to imbalances. The resonance modes were difficult to identify in the applied wheel speed range; therefore some additional tests are planned to increase the accuracy of the measurements.

1 Introduction

The majority of space missions today require a high pointing performance to obtain high-quality data from space. High-resolution Earth observation images, precise astronomical measurements or high-data rates by inter-satellite laser communications are a few examples that can be achieved with a high pointing precision and stability. The pointing stability is determined by the ability of the spacecraft to attenuate the different types of disturbances that are acting on the spacecraft. Low-frequency disturbances generally originate external to the spacecraft, resulting from sources such as aerodynamic drag, solar pressure, gravity gradient and magnetic gradient. High disturbances, on the other hand, generally originate from internal sources such as heat pumps or rotating wheels [1].

The low-frequency (external) disturbances (< 1Hz) can easily be corrected for by the Attitude Determination & Control System (ADCS). This spacecraft subsystem determines the orientation – also referred to as attitude – by means of a set of sensors and calculates the necessary action to be executed by a set of actuators, in order to maneuver the satellite to the desired attitude and stabilize it in this final orientation. The high-frequency (internal) disturbances (> 1Hz) cannot be eliminated by the ADCS itself, since the ADCS bandwidth is usually equal or less than 1 Hz. Other strategies therefore exist to reduce the effect on the pointing error of these high-frequency disturbances or 'jitter', such as a fine-steering mirror in the optical path of the payload and passive or active vibration isolation [1].

The largest contributors to the mechanical jitter onboard a spacecraft are considered to be the reaction wheels [2]. Reaction wheels are the prime actuators of the ADCS and primarily consist of a flywheel (a rotating mass) which is typically supported by a pair of ball bearings and driven by a brushless DC motor. The operating principle of a reaction wheel (or a momentum wheel) on a spacecraft is based on the conservation of momentum. By maintaining the flywheel at a rotational speed, a wheel provides momentum to the spacecraft. By varying the flywheel rotational speed, a reaction torque is generated. This reaction torque provides maneuvering or pointing capability to a spacecraft [3].

Although reaction wheels deliver high accuracy and agile pointing, these devices generate vibrations which are referred to as 'micro-vibration' because the resulting vibration on the satellite level is generally small, in the range of micro-g. These micro-vibrations are a combination of static and dynamic imbalances, motor disturbances, bearing irregularities or control errors (such as cogging and torque ripple) [4]. Taking into account that the pointing error is proportional to the root sum square of all disturbance amplitudes [5], it is of great importance to get a priori knowledge of the micro-vibrations of the reaction wheels to accurately predict the influence on the (optical) payload instruments and to take appropriate actions.

During the past 5 years, an entire ADCS with in-house made reaction wheels for CubeSats has been developed at the Department of Mechanical Engineering of the KU Leuven. CubeSats are small satellites that exists of one or more standardized units. One unit (1U) has dimensions of 10 x 10 x 10cm with a mass of about 1kg. Combining these units results in several derivatives such as (2U)- and (3U)- CubeSats. Compared to traditional satellites, this standardized type of spacecraft typically have shorter development cycles, smaller development teams, and, consequently, lower cost, both for the development and for the launch of the satellites. This low-cost access to space allowed universities and research institutes across the world to join the rapidly growing space community, while (inter)national space agencies recognized the potential of small spacecraft for (risk-taking) deep-space missions and technology demonstration missions. Today, however, small spacecraft are no longer seen as solely educational projects or technology demonstrators. Smallsats are making their way in almost every area of space: communication, remote sensing, science, and exploration.

In the remainder of the paper a study about the KU Leuven reaction wheel micro-vibrations will be discussed. In section 2, the current and future KU Leuven reaction wheel designs are explained. In section 3, a micro-vibration model of the KU Leuven reaction wheel will be presented together with some first estimates about the structural eigenmodes. In section 4, the micro-vibration tests are explained and the results are being analyzed and discussed. Finally, in section 5, the main results are summarized and the next steps to further improve the micro-vibration tests are considered.

2 KU Leuven reaction wheel design

In this section, the current and future KU Leuven reaction wheel designs are discussed. Driving factors for the current design were simplicity and affordability, which resulted in a sub-optimal reaction wheel performance. Secondly, the new or future design will be discussed to highlight the main adaptions with respect to the current design.

2.1 Current design

In this section the KU Leuven reaction wheel design is briefly presented. This design has outer dimensions of 40x40x28mm and a mass of 80g [6]. Its performance is characterized by the available motor torque of 0.5mNm and the theoretical maximal rotation speed of 10 000rpm. A cutout drawing of the KU Leuven reaction wheel is illustrated in Figure 1.

The total design exists of a brushless DC motor, a compact Oldham coupling, the rotor or flywheel, two radial bearings, and an upper and lower housing.

A **brushless DC motor** is used because of its high reliability and efficiency. The motor we use is the Faulhaber 1509T006, which has a flat design and delivers a torque up to 0.5mNm. The vacuum compatible version with an extended temperature range of -40 to 85C, was used to make the motor resilient to the space environment.

The motor is connected to the rotor by means of a **compact Oldham coupling**. This type of coupling is composed of three parts: one attached to the motor axis, one incorporated in the rotor design, and a middle

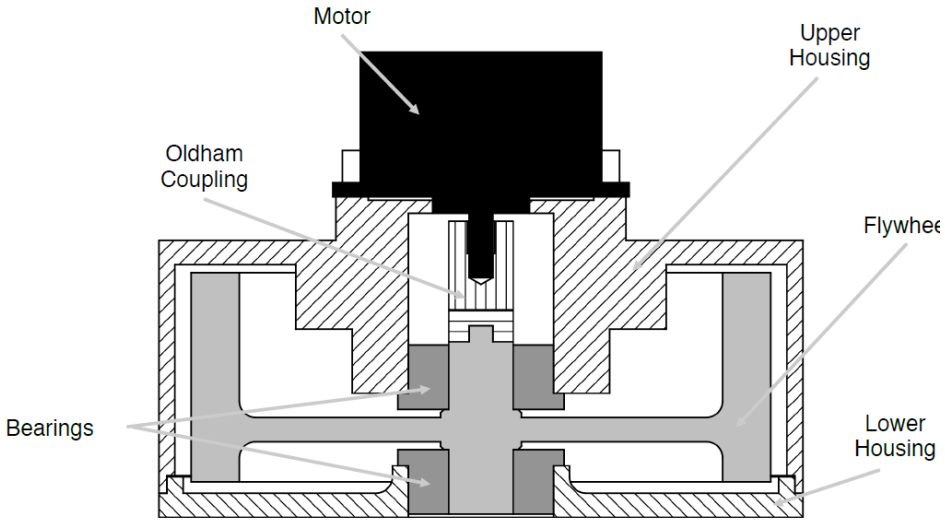

Figure 1: Cutout of the current reaction wheel design

part in between. This latter part is made of bronze for its excellent gliding properties and has two grooves that are perpendicular to each other and that mate with the other two coupling components.

The **rotor or flywheel** is optimized to have a high momentum for a low weight. It is precision machined out of stainless steel. Although a spoken rotor design would reduce the mass slightly, we opted for a full flange motor because it reduces the inherent imbalance and is produced more easily.

The rotor is supported by **two deep-groove ball bearings**. These bearings were preferred since they possess low friction torque thanks to their low contact surface, and are compact. For the bearing lubrication, special precautions must be taken due to the vacuum environment the reaction wheels will operate in. A vacuum-compatible grease was selected, with the downside of higher resulting friction. A flanged design was chosen to reduce the space needed for integration, because it adds stiffness compared to a snap ring fixture and because it facilitates the manufacturing of the reaction wheel housing.

Alternative bearing designs were also considered in [7]. Fluid and/or gas bearings are typically characterized by a high lifetime and low vibrations, but were ruled out due to the need for a pressurized lubricant or gas, which is not preferred in spacecraft. Magnetic bearings, on the other hand, are extremely complex and power demanding.

Finally, the **upper and lower housing** support the entire structure. The motor and bearings are mounted respectively on and in this structure and it interfaces with the structure of the satellite.

Three sets of 3 reaction wheels were already manufactured and assembled according to this design. Two reaction wheels of the total of 9 were used for the micro-vibrations tests as discussed in section 4.

2.2 Future design

The downside of using COTS components for the design of the reaction wheel is the dependency on existing products, which make it difficult to fully optimize the reaction wheel performance. The main disadvantages of the current design are the sub-optimal torque-speed characteristic of the Faulhaber brushless DC motor together with the necessary (Oldham) coupling, and the radial bearings which cannot support axial loads.

Therefore the KU Leuven is working on a new design based on the out-runner principle, as shown in Figure 2. In this design, the Faulhaber motor on top of the housing is replaced by a stator with carefully placed windings, while the flywheel, foreseen with magnets, is acting as the rotor. This avoids the coupling with respect to the current design. Furthermore, the motor torque-speed characteristic can be optimized over the desired speed range.

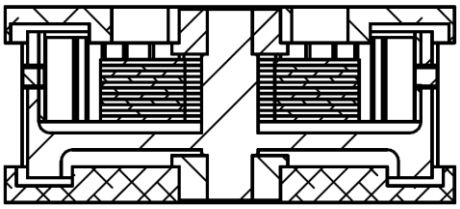

Figure 2: Cutout of the new reaction wheel design

Finally, angular bearings are considered instead of the previous chosen deep-groove ball bearings in order to reduce the micro-vibrations. This change is important especially for sensitive science missions on small spacecraft.

This outrunner reaction wheel is still under development and consequently no reaction wheels were already manufactured according to this new design.

3 KU Leuven reaction wheel micro-vibration model

The micro-vibration model of the KU Leuven reaction wheel introduced in this section is a combination of a structural dynamic model (theoretical model) and a disturbance model (empirical model). The proposed micro-vibration model is built based on the theoretic of rotor dynamics [8] and the models from [2] and [3]. For this model the following assumptions were made:

- The flywheel is assumed to be a rigid body within the frequency region of interest
- Gravity is not included (it does not affect the structural modes of the system)
- The micro-vibration model does not necessarily represent all structural modes of the complete reaction wheel assembly; the modes related to internal constructions, e.g. the coupling, are not taken into account

3.1 Structural dynamic model

For the structural dynamic model, the flywheel or rotor is modelled as a rigid disk supported by two radial bearings which are modelled each as a spring-damper system connected to the ground, as illustrated in Figure 3.

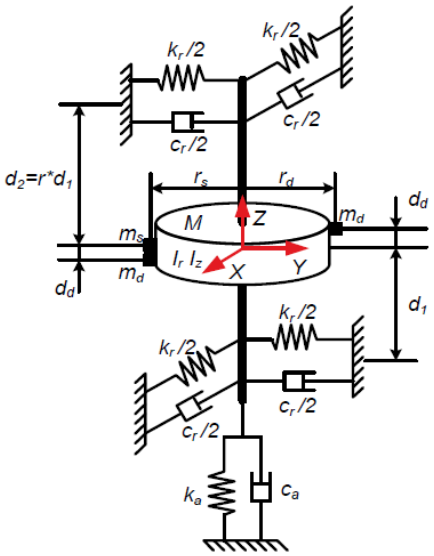

Figure 3: Illustration of the structural dynamic model [3]

The equations of motion can be derived using the Lagrange method for 5 degrees of freedom $q = \{x, y, z, \theta, \phi\}$, since the sixth degree (rotation about the z-axis) represents the motor torque and is not considered in the micro-vibration model. With m the mass of the rotor, I_r and I_z the moment of inertia for the radial and axial direction respectively, k_r and k_a the bearing stiffness in the radial and axial direction respectively, c_r and c_a the bearing damping coefficients in the radial and axial direction respectively, d_1 and d_2 the distances between the rotor's center of mass and the lower and upper bearing respectively, and the relative position $r = d_2/d_1$ of the rotor disk between the two bearings, and assuming that the rocking motions θ and ϕ have a small amplitude, these equations of motion can be further linearized to form the compact matrix Equation 1. The entire derivation of this equation can be found in [8].

$$\mathbf{M}\ddot{q} + \mathbf{C}(\Omega)\dot{q} + \mathbf{K}q = 0 \tag{1}$$

with,

$$q = \begin{Bmatrix} x \\ y \\ z \\ \theta \\ \phi \end{Bmatrix}, \qquad \mathbf{M} = \begin{bmatrix} m & 0 & 0 & 0 & 0 \\ 0 & m & 0 & 0 & 0 \\ 0 & 0 & m & 0 & 0 \\ 0 & 0 & 0 & I_r & 0 \\ 0 & 0 & 0 & 0 & I_r \end{bmatrix}$$

$$\mathbf{C}(\Omega) = \begin{bmatrix} c_r & 0 & 0 & 0 & \frac{1}{2}c_r d_1(1-r) \\ 0 & c_r & 0 & \frac{1}{2}c_r d_1(1-r) & 0 \\ 0 & 0 & c_a & 0 & 0 \\ 0 & 0 & \frac{1}{2}c_r d_1(1-r) & \frac{1}{2}c_r d_1^2(1+r^2) & -\Omega I_z \\ \frac{1}{2}c_r d_1(1-r) & 0 & 0 & \Omega I_z & \frac{1}{2}c_r d_1^2(1+r^2) \end{bmatrix}$$

$$\mathbf{K} = \begin{bmatrix} k_r & 0 & 0 & 0 & \frac{1}{2}k_r d_1(1-r) \\ 0 & k_r & 0 & \frac{1}{2}k_r d_1(1-r) & 0 \\ 0 & 0 & k_a & 0 & 0 \\ 0 & 0 & \frac{1}{2}k_r d_1(1-r) & \frac{1}{2}k_r d_1^2(1+r^2) & 0 \\ \frac{1}{2}k_r d_1(1-r) & 0 & 0 & 0 & \frac{1}{2}k_r d_1^2(1+r^2) \end{bmatrix}$$

With this proposed structural dynamic model, it is already possible to predict the resonant frequencies as a function of rotor speeds Ω when neglecting the damping of the system (i.e. $c_r = c_a = 0$). The frequency of the axial mode can directly be calculated by Equation (1). The frequencies of the translational and rotational mode can be calculated by numerically solving Equation (2), which is obtained by re-writing Equation (1) with the help of the complex coordinate method. It has 4 real roots, two of which are positive.

$$\omega^4 - \left(\frac{\Omega I_z}{I_r}\right)\omega^3 - \left(\frac{k_r}{m} + \frac{(1+r)^2 k_r d_1^2}{2I_r}\right)\omega^2 + \left(\frac{\Omega k_r I_z}{m I_r}\right)\omega + \left(\frac{(1+r)^2 k_r^2 d_1^2}{4 m I_r}\right) = 0 \tag{2}$$

A Campbell diagram is then the most common way to illustrate these resonant frequencies. In Figure 4 the Campbell diagram with the predicted resonance frequencies of the KU Leuven reaction wheel is illustrated for which the parameters from Table 2 were used. From this figure, an axial mode of around 1365Hz, a rocking mode of 311Hz, and a translational mode of 687Hz are expected at standstill and are summarized in Table 1.

Mode	Calculated frequency
Radial	1365
Axial	687
Rocking	311

Table 1: Calculated/predicted eigenfrequencies at standstill ($\omega = 0$rpm) of the KU Leuven reaction wheel

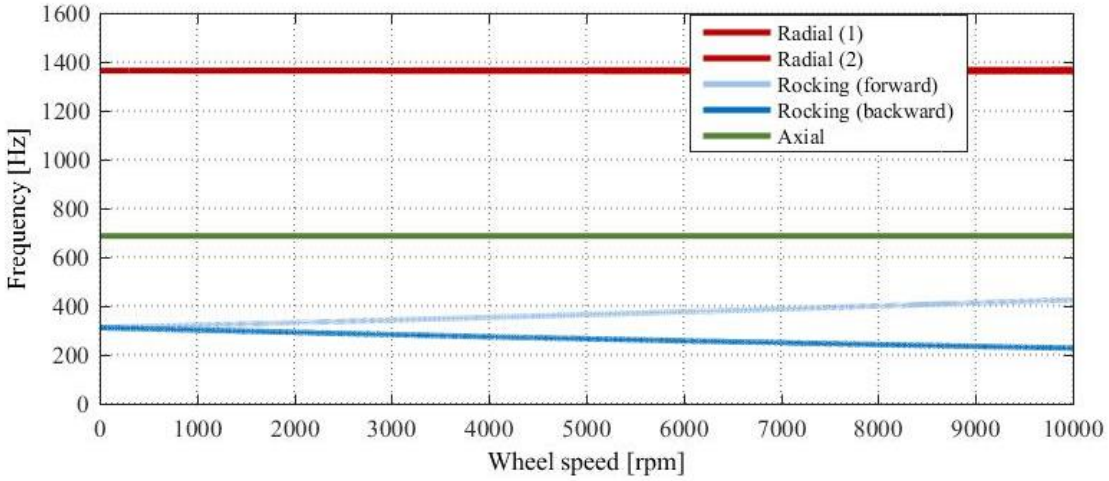

Figure 4: Campbell diagram with the calculated resonance modes of the KU Leuven reaction wheel assembly

The influence of the wheel speed on the rocking mode is clearly visible. The two diverging frequencies are called the forward and backward whirl. For the frequencies at 1365Hz this divergence is less pronounced, considering them as one (radial) translational mode.

Parameter	Value	Obtained from
I_z [kg m²]	$9.594 \cdot 10^{-12}$	CAD model
I_r [kg m²]	$7.778 \cdot 10^{-12}$	CAD model
m [kg]	$40.82 \cdot 10^{-3}$	CAD model
d_1 [m]	$5.75 \cdot 10^{-3}$	Technical drawing
d_2 [m]	$0.75 \cdot 10^{-3}$	Technical drawing
r [-]	0.13	Calculation ($= d_2/d_1$)
k_r [N/m]	$2.9 \cdot 10^{6}$	Estimation [11]
k_a [N/m]	$0.76 \cdot 10^{6}$	Estimation [11]

Table 2: Parameters used for the micro-vibration model of the KU Leuven reaction wheel

The resonance frequencies of the reaction wheel assembly should also be visible in the resulting waterfall plots from the micro-vibration tests. The predicted/calculated values from table can therefore be used as a reference value to easier distinguish them from the unavoidable noise in the test results.

3.2 Disturbance model

In the previous section, a structural dynamic model was proposed and the resonance frequencies were predicted by means of this model. In this model, however, the right-hand side of the equation was considered to be zero. In reality, micro-vibrations are induced by the reaction wheel assembly which can be categorized into fundamental sub and/or higher harmonic disturbances. The fundamental harmonic disturbances are considered to be the most significant micro-vibration source and are caused by the static

and dynamic imbalances of the flywheel. The sub/higher harmonic disturbances are caused by irregularities in the reaction wheel assembly, such as bearing imperfections.

The static unbalance U_s can be expressed in two ways: (1) by means of an additional small mass m_s at a distance r_s from the rotor's center of mass as illustrated Figure 3, or (2) by means of the total mass of the rotor m which experience a certain eccentricity ε due to limited manufacturing capabilities. Equation (3) formulates both expressions. The static imbalance is typically given in g-mm.

$$U_s = m_s r_s = m\varepsilon \tag{3}$$

In the same way, the dynamic imbalance U_d can be expressed in two ways: (1) by means of two additional small masses m_d on a distance r_d from the rotor's center of mass and an axial distance d_d in between them as illustrated in Figure 3, or (2) by means of the total axial inertia of the rotor I_z which experience a certain angular error χ due to limited manufacturing capabilities. Equation (4) formulates both expressions. The dynamic imbalance is typically given in g-mm².

$$U_d = 2m_d r_d d_d = I_z \chi \tag{4}$$

Since all components of the KU Leuven reaction wheels were manufactured with certain tolerances, the worst case can be calculated for both imbalances (assuming the tolerances were met during manufacturing). In Table 3 the worst case imbalance were calculated according to the tolerances of the design.

Imbalance	Maximum error	Maximum imbalance
Static	$\varepsilon = 40\mu m$	$U_s = 1.6$g-mm
Dynamic	$\chi = 6.2$mrad	$U_d = 59$g-mm²

Table 3: The maximum predicted imbalances according to the KU Leuven reaction wheel design tolerances

The excitation of both imbalances can now be added to Equation (1) to obtain the full micro-vibration model. In addition to the imbalance disturbances at the fundamental harmonic ($h = 1$), the disturbances due to irregularities in the reaction wheel assembly are also added at other harmonics ($h \neq 1$).

$$\mathbf{M}\ddot{q} + \mathbf{C}(\Omega)\dot{q} + \mathbf{K}q = U_{im}(\Omega t) + U_{irr}(h\Omega t) \tag{5}$$

with,

$$U_{im}(\Omega t) = \begin{Bmatrix} -U_s\Omega^2 \sin(\Omega t) \\ U_s\Omega^2 \cos(\Omega t) \\ 0 \\ U_d\Omega^2 \cos(\Omega t) \\ U_d\Omega^2 \sin(\Omega t) \end{Bmatrix}, \qquad U_{irr}(h\Omega t) = \begin{Bmatrix} -\sum_i^{n_f} U_i^f \Omega^2 \sin\left(h_i^f \Omega t + \beta_i^f\right) \\ \sum_i^{n_f} U_i^f \Omega^2 \cos\left(h_i^f \Omega t + \beta_i^f\right) \\ 0 \\ \sum_i^{n_t} U_i^t \Omega^2 \cos\left(h_i^t \Omega t + \beta_i^t\right) \\ \sum_i^{n_t} U_i^t \Omega^2 \sin\left(h_i^t \Omega t + \beta_i^t\right) \end{Bmatrix}$$

where U_i are the harmonic amplitudes of ith harmonic, h_i is the ith harmonic number, and β_i is a random phase angle.

The left-hand side of Equation (5) should be similar for reaction wheels made according to the same design, while the right-hand side is unique for each reaction wheel, since this part of the equation depends on the actual eccentricity and bearing irregularities.

4 Micro-vibration testing

The aim of the micro-vibration tests are two-fold: (1) to validate the micro-vibration model as described in the previous section (in order to be able to accurately define the effect on the pointing system of a spacecraft structure), and (2) to evaluate the quality of the manufacturing and assembly of the KU Leuven reaction wheels. This can be done based on the so-called waterfall plots, which can be created from the micro-vibration test data.

In this section, first the test setup will be described, next the test procedure that is applied and the processing of the data, and finally the test results are analyzed and discussed.

4.1 Test setup

4.1.1 Data acquisition

The total test setup is illustrated in Figure 5. One of the KU Leuven reaction wheels was mounted on a measuring cell via an aluminum reaction wheel mounting plate. The measuring cell itself was rigidly mounted on an air table.

For the measuring cell, the Kistler Dynamometer, type 9119AA1, was chosen. This dynamometer consists of four 3-component piezo-electric force sensors mounted under high preload between a cover plate and two lateral base plates. The force sensor current signals were further converted into a proportional voltage signal by the Kistler multichannel charge amplifier, type 5070A. The 6 amplified signals (3 forces and 3 torques) of the amplifier were finally sampled by a LMS acquisition system at a rate of 3200Hz. A 10N/V and a 1Nm/V setting was applied for the three forces and three torques respectively.

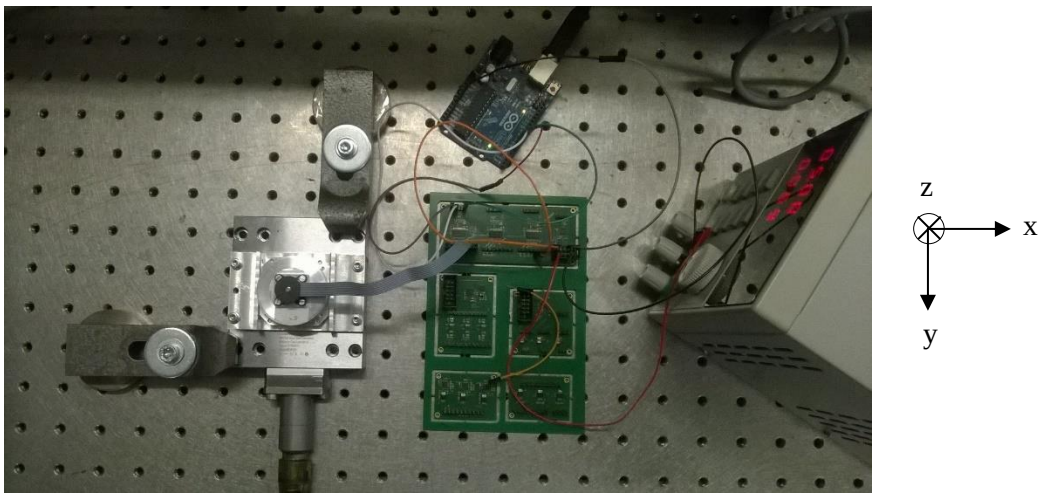

Figure 5: Illustration of the micro-vibration test setup

4.1.2 Frequency range of the test setup

It is important to only measure the reaction wheel vibrations. Therefore, the Kistler dynamometer was rigidly mounted on a Newport RS2000 air table to isolate the dynamometer from ambient seismic

vibrations (< 10Hz). Furthermore, the first resonance of the test setup itself was measured to be around 2000 Hz, using an impact hammer while measuring the forces of the dynamometer. The force/force (dynamometer/hammer) transmissibility curve of these impact measurements is illustrated in Figure 6 for the three directions (according to the axes as illustrated in Figure 5). From these data, the characterization of the wheels was thus limited to be within the range of 10 and <2000Hz.

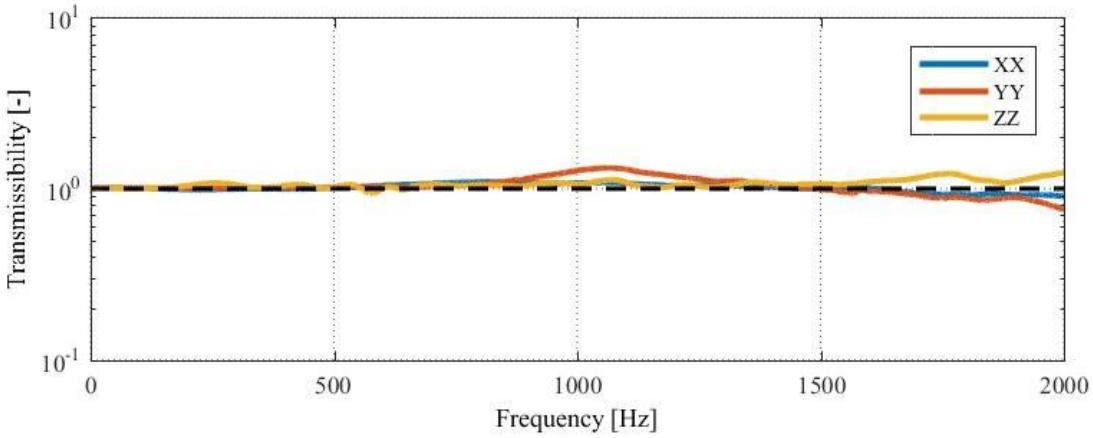

Figure 6: The measured transmissibility (force-to-force) of the impact test to determine the characterization frequency range

4.2 Test procedure

Two of the KU Leuven reaction wheels were used for the micro-vibration tests. Through the remainder of this paper, these reaction wheels will be defined as RW1 and RW2. Although both wheels have the same design, they were made by two different manufacturers.

In order to acquire the desired waterfall plots, the forces and torques need to be measured over the entire wheel speed range. Since the micro-vibration model, as proposed in Section 3, is only valid for steady-state conditions, the wheel speed should be constant over the measuring period at each wheel speed.

Two different approaches are usually applied to get these data with steady-state conditions: (1) by taking measurements at each wheel speed separately (with an increase in wheel speed between two consecutive measurements), or (2) by performing a spin-down of the reaction wheel where the time history of the measurement data can be subdivided into quasi steady-state time slices. For the latter option, it is assumed that the friction torque in the reaction wheel is very low, such that the wheel speed slowly decreases over time, and the wheel speed can be considered as steady-state over each time slice. Since the tested KU Leuven reaction wheels have relatively large friction torque, the first option has been chosen for obtaining the time history.

The wheel speed was increased from 0rpm to 2000rpm in steps of 50rpm for each wheel. After each 30s, the wheel speed was commanded to increase, resulting in a total measuring time of 1230s or 21.5min, as illustrated in Figure 7 for RW1.

The KU Leuven reaction wheels are driven by means of a PWM-signal and an encoder gives back the real wheel speed. The wheel speeds were controlled by a simple PID controller based on the rate feedbacks. A power supply provided the necessary supply voltage to the motors of the reaction wheels.

Since the wheel speed control and the vibration measurements were not commanded from one platform, these two data sets (wheel speed measurements and vibration measurements) are inherently not synchronized. The synchronization is discussed in the next section.

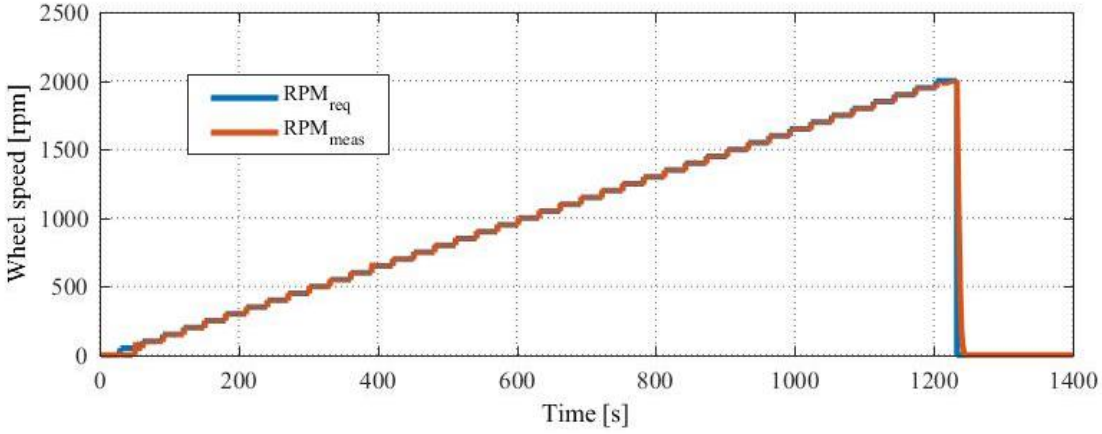

Figure 7: The wheel speed profile of RW1 during the entire micro-vibration test
(blue: required wheel speed, red: measured wheel speed)

4.3 Test data processing

The obtained dynamometer data were loaded into Matlab and processed first. The processing steps are illustrated in Figure 8.

Figure 8: Illustration of the processing steps in Matlab

First, the measured moments M_m^{DF} in the dynamometer frame were compensated for the offset between the reaction wheel center and the reference frame of the dynamometer according to Equation (6), with F_m^{DF} the measured forces and v^{DF} the offset vector from the origin of the dynamometer to the center of the reaction wheel, both in the dynamometer frame (DF).

$$M = M_m^{DF} - v^{DF} \times F_m^{DF} \tag{6}$$

Next, a 7th order Butterworth filter was applied on the data with a cutoff frequency of 1500Hz. Subsequently, the speed and vibration data were visually synchronized. Since the wheel speed was increased each 30s, a small increase in amplitude should be identified in the vibration data for each axis, which is illustrated in Figure 9.

Finally, a Hanning window was applied on a small time period of 10s at each wheel speed while executing the Fast Fourier Transformation (fft) to transform the time data to the frequency domain.

In each time period of 30s, the wheel speed increases relatively fast to the required wheel speed (< 5s). Taking into account a time period of about 10s to ensure the dynamic behavior of the system has damped out, and a safety margin of 5s synchronization uncertainty, the Hanning window was applied over the data from each 15th to 25th second at each wheel speed. This is clearly visualized in Figure 10.

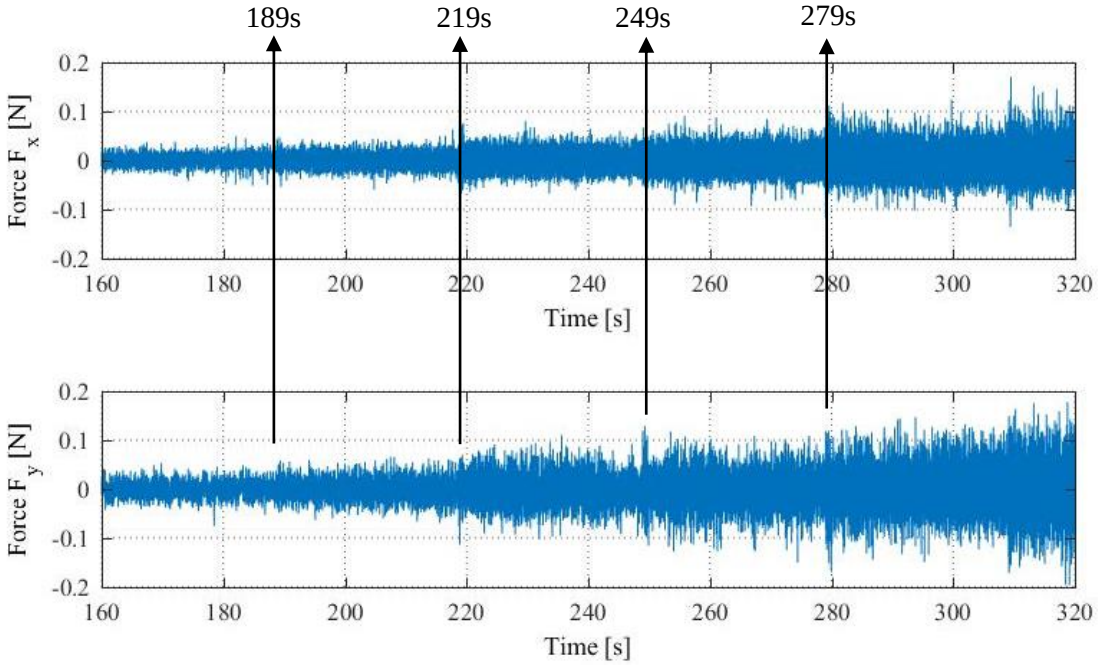

Figure 9: Illustration of the visual synchronization procedure; an increase in amplitude is identified for both force signals of RW1 at the same time with a 30s time interval in between

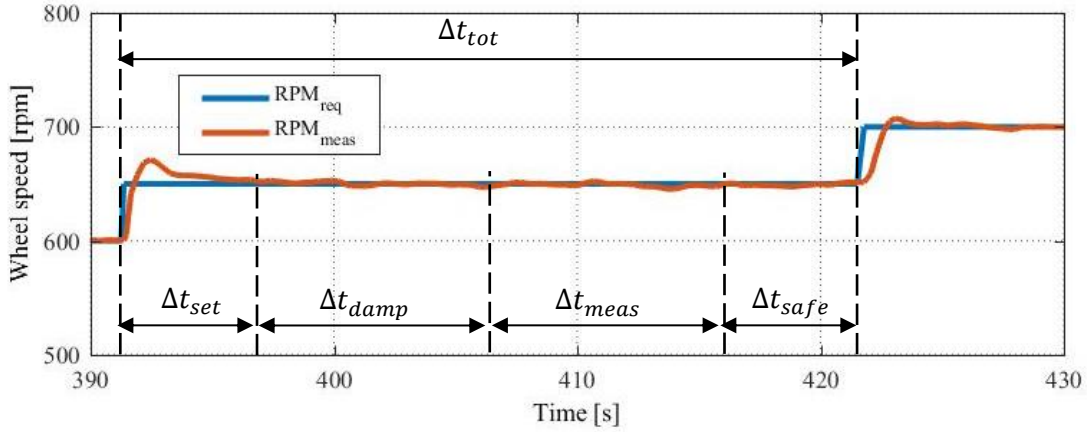

Figure 10: Illustration of the time periods per wheel speed on a detail of Figure 7 for RW1, with $\Delta t_{tot} =$ 30s the total time period per required wheel speed, $\Delta t_{set} <$ 5s the settling time, $\Delta t_{damp} =$ 10s the time to damp out the dynamics of the system, $\Delta t_{meas} =$ 10s the actual time period used to calculate the spectrum, and $\Delta t_{safe} =$ 5s the safety margin on the synchronization uncertainty.

4.4 Test results

By grouping the calculated spectra of each wheel speed together, the waterfall plots can be generated for each signal. The amplitude density spectra (ASD) for RW1 and RW2 are shown in Figure 11 and Figure 12.

For both wheels, some general conclusions can be made first. As expected, the spectra for the x- and y-forces and moments are almost the same. Furthermore, the z- moment is negligible compared to the other two moments, since this is the driven torque of the motor.

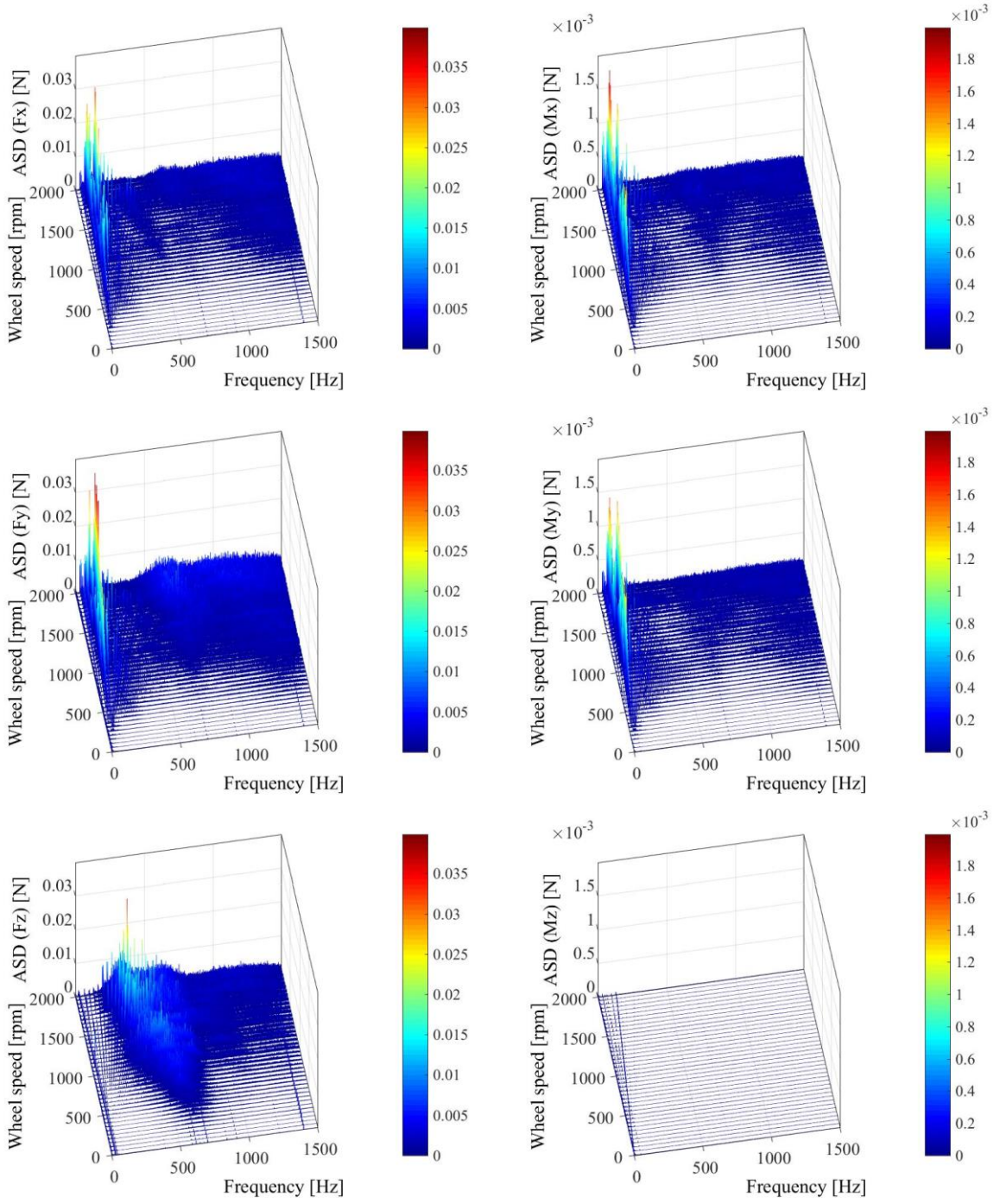

Figure 11: Amplitude Density Spectra (ASD) for RW1

Specifically for RW1, the ASD waterfall plots from Figure 11 are difficult to interpret. In the range of 500 to 1500Hz (above about 800rpm), broadband noise can be seen. This can be credited to a loose part that was shaking. During assembly of the bearings in the reaction wheel housings, it was noticed that the intentional tight fit couldn't be attained due to the fact that the tolerances were not met by the manufacturer. Furthermore, the second harmonic is the largest peak value, and not the first harmonic as expected, which means that the bearings experience some misalignment with respect to each other. The large forces in the z-axis supports this hypothesis, according to [10].

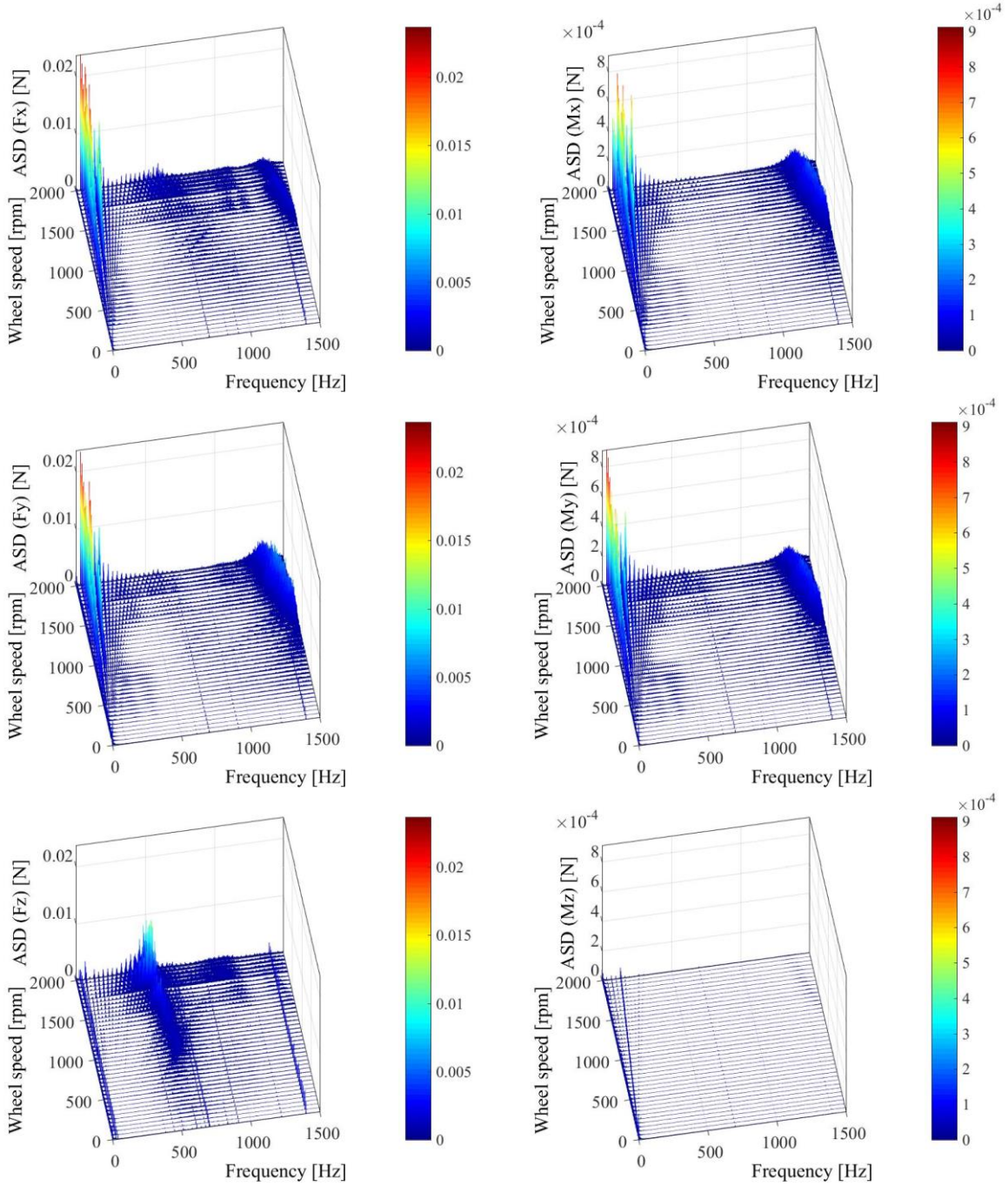

Figure 12: Amplitude Density Spectra (ASD) for RW2

Better results (i.e. as expected) are obtained for RW2, as can be seen in Figure 12. For this reaction wheel, made by a different manufacturer, the first harmonic is the largest peak value, originating from the unavoidable imbalance. Furthermore, a strong amplification is seen around 650Hz, mainly in the Fz-signal. Comparing to the results of the micro-vibration model of section 3.1, this amplification could correspond to the axial mode, which was calculated to be around 687Hz. Also some amplifications are seen in the higher frequency regions around 1300 – 1500Hz. It seems to be the back whirl of the rocking mode, which does not correspond to the predicted values of the micro-vibration model.

Based on the measured amplitudes of the forces and moments at the first harmonic, the static and dynamic imbalances can be calculated according to Equation (5), respectively. At the highest wheel speed (2000

rpm), the highest signal-to-noise is obtained for this calculation. The results for RW2 are listed in Table 4 together with the maximum predicted imbalances of Table 3. The measured imbalances are 3 times smaller than the maximum predicted imbalances and are in the magnitude range of comparable CubeSat reaction wheels commercially available [6].

Imbalance	Maximum imbalance	Measured imbalance
Static	$U_s = 1.6$g-mm	$U_s = 0.5$g-mm
Dynamic	$U_d = 59$g-mm²	$U_d = 20$g-mm²

Table 4: Measured imbalances based on the force and moment amplitudes at the first harmonic.

5 Conclusion

In this paper, the need to accurately characterize the reaction wheel behavior is explained first where after the KU Leuven reaction wheel design was given. A micro-vibration model, which was a combination of a theoretical structural dynamic model and an empirical disturbance model, was proposed to predict the resonance modes and the imbalances of the KU Leuven reaction wheels. Finally, the performed micro-vibration tests were discussed and the results were analyzed.

5.1 Future considerations

Since the generated waterfall plots from these first micro-vibration tests were difficult to interpret, such that the predictions of the micro-vibration model could not be verified, more tests are planned. Some considerations are already summarized here in order to increase the quality of the measurement data:

- If possible, the wheel speed should be controlled from the same software platform (e.g. LMS) to avoid the synchronization problem
- If possible, the wheel speed limit should be increased from 2000rpm to at least 4000rpm or higher. At higher speeds, the resonance amplifications are more pronounced and the signal-to-noise ratio will increase.
- If possible, longer time periods (> 30s) can be taken at each wheel speed, e.g. 60s. This of course doubles the total measurement time, but allows to make more than one spectrum and to average these spectra.

Acknowledgements

Strategic Basic (SB) PhD fellow at Research Foundation – Flanders (FWO).

References

[1] J. Vandersteen, *Observation and Estimation for spac*e, PhD thesis, KU Leuven, Belgium (2012).

[2] R. A. Masterson, *Development and Validation of Reaction Wheel Disturbances Models: Empirical Model, Journal of Sounds and Vibration*, Vol. 249, pp. 5757-598 (2002).

[3] P. Le, *Micro-disturbances in reaction wheels*, PhD thesis, TU Eindhoven, The Netherlands (2017).

[4] D. Kim, *Micro-vibration model and parameter estimation method of a reaction wheel assembly*, Journal of Sound and Vibration, Vol. 333, No. 4 (2012).

[5] M. J. Sidi, *Spacecraft Dynamics and Control*, Cambridge University Press (1997).

[6] T. Delabie, R. Boonen, D. Vandepitte, *Building, Testing and Analyzing Robust and Accurate CubeSat Reaction Wheels*, in *Proceedings of The 10th International ESA Conference on Guidance, Navigation & Control Systems, Salzburg, Austria, 2017 May 29 – June 2*, Salzburg (2017).

[7] J. Goyvaerts, *Design and Implementation of a low-cost Attitude Determination and Control System for CubeSats*, MSc thesis, Dept. Mech. Eng., KU Leuven, Belgium (2011).

[8] G. Genta, *Dynamics of rotating systems*, Springer – Mech. Eng. Series (2005).

[9] J. Shields, et al., Characterization of CubeSat Reaction Wheel Assemblies, in Journal of Small Satellites, Vol. 6, No. 1, Deepak Publishing (2017), pp. 565-580.

[10] W. Heylen, S. Lammens, P. Sas, *Modal Analysis Theory and Testing*, Katholieke Universiteit Leuven, Departement Werktuigkunde, Leuven (1997).

[11] E. P. Gargiulo Jr, *A simple way to estimate bearing stiffness*, article in Machine Design (1980).